Formation and decay of resonance states in ^{9}Be and ^{9}B nuclei: Microscopic three-cluster model investigations

V. S. Vasilevsky*
Bogolyubov Institute for Theoretical Physics, Kiev 03143, Ukraine

K. Katō†
Nuclear Reaction Data Centre, Faculty of Science, Hokkaido University, Sapporo 060-0810, Japan

N. Zh. Takibayev‡
Al-Farabi Kazakh National University, Almaty 050040, Kazakhstan

(Received 10 April 2017; revised manuscript received 4 August 2017; published 25 September 2017)

We study the nature of the low-lying resonance states in mirror nuclei ^{9}Be and ^{9}B. Investigations are performed within a three-cluster model. The model makes use of the hyperspherical harmonics, which provides a convenient description of the three-cluster continuum. The dominant three-cluster configurations $\alpha + \alpha + n$ and $\alpha + \alpha + p$ in ^{9}Be and ^{9}B, respectively, are taken into account. Dominant decay channels for all resonance states in ^{9}Be and ^{9}B are explored. Much attention is paid to the controversial $1/2^{+}$ resonance states in both nuclei. We study effects of the Coulomb interaction on the energy and width of three-cluster resonances in the mirror nuclei ^{9}Be and ^{9}B. We also search for the Hoyle-analog state, which is a key step for alternative ways to synthesize ^{9}Be and ^{9}B in triple collisions of clusters in a stellar environment.

DOI: 10.1103/PhysRevC.96.034322

I. INTRODUCTION

The resonance state is one of the challenging problems for theoretical physics, as well as for nuclear physics. There are common features of resonance states observed in a few- or many-channel systems. However, there are some specific features related to ways of the excitation or generation of resonance states and to ways of the decay of nuclear resonance states. It is well known that some resonance states are observed in one set of reactions and do not manifest themselves in another set of reactions. Special attention is attracted to the resonance states formed by three interacting clusters, i.e., resonance states embedded in the three-cluster continuum. Such resonance states have been repeatedly observed in nuclei that have well-determined three-cluster structures. This result suggests that bound states and many resonance states lie below and above, respectively, the threshold of the three-cluster continuum. In other words, bound states and a large part of resonance states in three-cluster nuclei are generated by an interaction of three clusters. As examples of such nuclei, we mention ^{5}H, ^{6}He, ^{6}Be, ^{9}Be, ^{9}B, and so on.

In the present paper, a microscopic three-cluster model will be used to study the nature of resonance states in ^{9}Be and ^{9}B. The dominant three-cluster configurations $\alpha + \alpha + n$ and $\alpha + \alpha + p$ are selected to describe the low-excitation energy region in these nuclei. The microscopic model formulated in Ref. [1] makes use of harmonic oscillator functions to describe the intercluster motion. The model is called AM HHB, which stands for the algebraic three-cluster model with the hyperspherical harmonics basis. The first application of this model to study the resonance structure of ^{9}Be and ^{9}B was made in Ref. [2]. Results presented in Ref. [2] were obtained with the Minnesota potential (MP). In the present paper, we use the modified Hasegawa-Nagata potential (MHNP) [3,4] and will show a very good correspondence between calculations and experiments. Based on this successful result, we pay much more attention to the $1/2^{+}$ resonance states and the Coulomb effects on the resonance states in mirror nuclei. In addition, we search for the Hoyle-analog states in ^{9}Be and ^{9}B.

There are many attempts to study the resonance structure of ^{9}Be and ^{9}B within various methods and models [5–13]. Those investigations have been dominantly performed within the cluster model and different variants of the resonating group method. In some cases, the determination of resonance parameters is carried out in the framework of models, where the three-cluster problem is reduced to a many-channel two-body system by representing ^{9}Be (^{9}B) as coupled-channel systems of $^{8}\mathrm{Be} + n$ ($^{8}\mathrm{Be} + p$) and $^{5}\mathrm{He} + {}^{4}\mathrm{He}$ ($^{5}\mathrm{Li} + {}^{4}\mathrm{He}$). Other groups of papers take into account that all resonance states in ^{9}Be and ^{9}B belong to the three-cluster continuum. The position of resonance states and their properties have been determined by using the complex scaling methodology or the hyperspherical harmonics basis. The latter allows one to incorporate proper boundary conditions for decays of a three-cluster system into three independent clusters, while the former allows one to locate resonance states in the continuum of many-channel and many-cluster systems.

A special attention is attracted by the $1/2^{+}$ excited states in ^{9}Be and ^{9}B. This is stipulated by two factors. First, the position of these resonances was obtained at different energies in various experiments. Some experiments claimed that there are no such resonances in ^{9}Be or ^{9}B. Second, different theoretical investigations suggested different energies

*vsvasilevsky@gmail.com
†kato-iku@gd6.so-net.ne.jp
‡takibayev@gmail.com

and the nature of the $1/2^+$ excited states in ^{9}Be and ^{9}B. Some theoretical investigations stressed that there is no $1/2^+$ excited states in ^{9}Be and that the resonance peak in the reactions of photodisintegration is associated with a virtual state. Other groups of investigations detected the $1/2^+$ excited states in ^{9}Be and ^{9}B as resonance states in a two- or three-body continuum. This dispute also encouraged us to perform the present investigations.

In the last decade, light nuclei have been a subject for *ab initio* calculations, by using modern nucleon-nucleon potentials. These methods suggest a more advanced description of nuclear systems. The *ab initio* methods employing fundamental and realistic nucleon-nucleon interactions are, for instance, the no-core shell-model (NCSM) [14] and the quantum Monte Carlo method (QMCM) [15]. The NCSM employs a huge basis of oscillator functions to describe the relative motion of nucleons in a compound nuclear system. In Ref. [16], an advanced version of the model was formulated which combines NCSM and the resonating group method (it was called the NCSM/RGM model) to study the cluster-cluster scattering or decay of a nucleus onto two clusters. Another version of NCSM (NCSMC) was formulated in Ref. [17] to study a decay of compound nuclei into three fragments (clusters). NCSMC is similar to our model in respect of representing the asymptotic part of the wave functions of continuous spectrum states. The hyperspherical harmonics were used in Ref. [17] to represent the asymptotic part of wave functions and to implement proper boundary conditions. This method was successfully used in Refs. [18–20] to study the discrete and continuous spectra of ^{6}He. However, the nucleus ^{9}Be was investigated with another version of NCSM (NCSM/RGM), where the three-body continuum was modeled by the two-body $^8\mathrm{Be}+n$ configuration (see Refs. [19,21,22]). The contribution of the three-nucleon forces and their effects on the spectrum of the ground and resonance states in ^{9}Be were investigated in Ref. [23] in detail. Within QMCM in Ref. [23], the resonance states in ^{9}Be were treated as discrete states. It was shown in Ref. [23] that the spectrum of excited states and their relative position strongly depend on the shape of five realistic nucleon-nucleon potentials.

We mention the numerous experimental investigations of ^{9}Be and ^{9}B in Refs. [24–31], where the structure and different processes taking place in these nuclei have been investigated.

Our paper is organized in the following way. In Sec. II, we explain the key elements of our model. Main results are presented in Sec. III. A detailed discussion of the nature of $1/2^+$ resonance states is given in Sec. IV. In Sec. V, we study effects of the Coulomb interaction on the energies and widths of resonance states in ^{9}Be and ^{9}B. The quest for the Hoyle-analog states is presented in Sec. VI. We close the paper by summarizing the obtained results in Sec. VII.

II. MODEL FORMULATION

In this section, we shortly outline the main ideas of the model. We start with the wave function of a nucleus consisting of three clusters, as a key element of the model formulation. To describe a three-cluster system, one has to construct a three-cluster function,

$$\Psi_{JM_J}=\sum_{L,S}\widehat{\mathcal{A}}\big\{[[\Phi_1(A_1,s_1)\Phi_2(A_2,s_2)]\Phi_3(A_3,s_3)]_S \times f^{(J)}_{L,S}(\mathbf{x},\mathbf{y})\big\}_{JM_J}. \tag{1}$$

By solving a many-body Schrödinger equation, we have to determine the intercluster wave function $f^{(J)}_{L,S}(\mathbf{x},\mathbf{y})$ and the energies of bound states or S matrix for states of the continuous spectrum. The Jacobi vectors $\mathbf{x}$ and $\mathbf{y}$ determine the relative position of clusters. The wave functions $\Phi_\alpha(A_\alpha,s_\alpha)$ ($\alpha=1$, 2, 3) describing the internal motion of the cluster consisted of A_α nucleons and with the spin s_α are assumed to be fixed, and they possess some very important features—for instance, they are antisymmetric and translation invariant. The adiabaticity related to a fixed form of the wave functions $\Phi_\alpha(A_\alpha,s_\alpha)$, is the main assumption of the method, which is well known as the resonating group method [32]. In fact, the wave function (1) provides a projection operator, which reduces the many-particle problem to an effective three-body problem with a nonlocal energy-dependent potential (see details in Ref. [32]). For the amplitudes

$$f^{(J)}_{L,S}(\mathbf{x},\mathbf{y})=\sum_{l_1,l_2}f^{(J)}_{l_1,l_2;L,S}(x,y)\big\{Y_{l_1}(\widehat{\mathbf{x}})Y_{l_2}(\widehat{\mathbf{y}})\big\}_{LM_L}, \tag{2}$$

one can deduce an infinite set of two-dimensional integrodifferential equations (with respect to the variables x and y). This set of equations can be further simplified. If we introduce the hyperspherical coordinates

$$x=\rho\cos\theta,\quad y=\rho\sin\theta,\qquad \Omega=\{\theta,\widehat{\mathbf{x}},\widehat{\mathbf{y}}\} \tag{3}$$

and construct a full set of orthonormal hyperspherical harmonics

$$\mathcal{Y}_{K,l_1,l_2,LM_L}(\Omega)=\chi_{K,l_1,l_2}(\theta)\{Y_{l_1}(\widehat{\mathbf{x}})Y_{l_2}(\widehat{\mathbf{y}})\}_{LM_L} \tag{4}$$

(see the definition of hyperspherical harmonics, e.g., in [1,33]), then the wave function (1) takes the form

$$\Psi_{JM_J}=\widehat{\mathcal{A}}\Bigg\{\sum_{c=\{K,l_1,l_2;L,S\}}[[[\Phi_1(A_1,s_1)\Phi_2(A_2,s_2)]\Phi_3(A_3,s_3)]_S \times\mathcal{Y}_{K,l_1,l_2;L}(\Omega)]_{JM_J}\psi_{K,l_1,l_2;L,S}(\rho)\Bigg\}, \tag{5}$$

where the hyper-radial components $\psi_{K,l_1,l_2;L,S}(\rho)$ of the wave function obey an infinite set of integrodifferential equations. The last step toward a simplification of the numerical solutions of such a system of equations is to expand the hyper-radial amplitudes $\{\psi_{K,l_1,l_2;L,S}(\rho)\}$ in the basis of the hyper-radial part of oscillator functions in the six-dimensional space as

$$\psi_{K,l_1,l_2;L,S}(\rho)=\sum_{n_\rho}C_{n_\rho K,l_1,l_2;L,S}(b)R_{n_\rho,K}(\rho,b), \tag{6}$$

where $R_{n_\rho,K}(\rho,b)$ is an oscillator function,

$$R_{n_\rho,K}(\rho,b) = (-1)^{n_\rho}\mathcal{N}_{n_\rho,K}r^K \exp\left\{-\frac{1}{2}r^2\right\}L_{n_\rho}^{K+3}(r^2),$$
$$r = \rho/b, \quad \mathcal{N}_{n_\rho,K} = b^{-3}\sqrt{\frac{2\Gamma(n_\rho+1)}{\Gamma(n_\rho+K+3)}}, \qquad (7)$$

and b is the oscillator length.

The expansion of Ψ_{JM_J} in the oscillator basis reduces the set of integrodifferential equations to a system of linear algebraic equations for the expansion coefficients

$$\sum_{\widetilde{n}_\rho,\widetilde{c}}\{\langle n_\rho,c|\widehat{H}|\widetilde{n}_\rho,\widetilde{c}\rangle - E\langle n_\rho,c|\widetilde{n}_\rho,\widetilde{c}\rangle\}C_{\widetilde{n}_\rho,\widetilde{c}} = 0, \qquad (8)$$

where the multiple index c denotes a channel of the hyperspherical basis $c = \{K,l_1,l_2,L,S\}$. This system is relevant to bound states and to continuous spectrum states. To obtain a spectrum of bound states, one can use the diagonalization procedure for the reduced set of Eqs. (8). However, to find the wave functions and elements of the scattering S matrix, one has to implement proper boundary conditions for the expansion coefficients in Eq. (8). These conditions were thoroughly discussed in Ref. [1].

The completeness relations for hyperspherical harmonics and oscillator functions are

$$\sum_{K,l_1,l_2,LM}\mathcal{Y}_{K,l_1,l_2,LM}(\Omega)\mathcal{Y}_{K,l_1,l_2,LM}(\widetilde{\Omega}) = \delta(\Omega-\widetilde{\Omega}),$$
$$\sum_{n_\rho}R_{n_\rho,K}(\rho,b)R_{n_\rho,K}(\widetilde{\rho},b) = \delta(\rho-\widetilde{\rho}),$$

where the δ function $\delta(\Omega-\widetilde{\Omega})$ stands for the product of five δ functions for each of the hyperspherical angles $\{\theta,\widehat{\mathbf{x}},\widehat{\mathbf{y}}\} = \{\theta,\theta_{\mathbf{x}},\varphi_{\mathbf{x}},\theta_{\mathbf{y}},\varphi_{\mathbf{y}}\}$. The completeness relations ensure that, up to now, we made no restrictions or approximations. Approximations will be formulated later, when we proceed to numerical solutions of the system of Eq. (8).

Note that hyperspherical angles determine the shape and orientation in the space of a triangle connecting the centers-of-mass of interacting clusters. Thus, the hyperspherical harmonics describe all possible rotations and all possible deformations of the triangle. Each hyperspherical harmonic $\mathcal{Y}_{K,l_1,l_2,LM}(\Omega)$ (similar to the solid harmonics) predetermines one or several dominant shapes of the three-cluster triangles (see some illustrations for this statement in Refs. [34,35]).

As for the functions $\psi_{K,l_1,l_2;L,S}(\rho)$ and $R_{n_\rho,K}(\rho,b)$, they describe radial excitations or the monopole or breathing mode excitations. Besides, the wave functions $\psi_{K,l_1,l_2;L,S}(\rho)$ describe all elastic and inelastic processes in the three-cluster continuum and, thus, contain elements of the scattering S matrix:

$$\psi_{K,l_1,l_2;L,S}(\rho) \Rightarrow \delta_{c_0,c}\psi_c^{(-)}(k\rho,\eta_c) - S_{c_0,c}\psi_c^{(+)}(k\rho,\eta_c), \qquad (9)$$

where c_0 and c denote the incoming and present or outgoing channels, respectively; in general, they involve five quantum numbers $c = \{K,l_1,l_2,L,S\}$. Six-dimensional incoming $\psi_c^{(-)}(k\rho,\eta_c)$ and outgoing $\psi_c^{(+)}(k\rho,\eta_c)$ waves are determined as follows:

$$\psi_c^{(\pm)}(k\rho,\eta_c) = W_{\pm i\eta_c,K+2}(2ik\rho)/\rho^{5/2}, \qquad (10)$$

where $W_{\nu,\mu}(z)$ is the Whittaker function (see Chap. 13 of Ref. [36]), and η_c is the Sommerfeld parameter

$$\eta_c = \frac{m}{\hbar^2}\frac{Z_{c,c}e^2}{k}.$$

The wave functions $\psi_c^{(\pm)}(k\rho,\eta_c)$ are solutions of the differential equations

$$\left\{-\frac{\hbar^2}{2m}\left[\frac{d^2}{d\rho^2}+\frac{5}{\rho}\frac{d}{d\rho}-\frac{K(K+3)}{\rho^2}\right]+\frac{Z_{c,c}e^2}{\rho}-E\right\}$$
$$\times\,\psi_c^{(\pm)}(k\rho,\eta_c) = 0, \qquad (11)$$

where $Z_{c,c}e^2/\rho$ represents the effective Coulomb interaction in hyperspherical coordinates. It should be stressed that Eq. (11) and the Coulomb interaction in this equation represent the asymptotic form of the microscopic three-cluster Hamiltonian, when the distances between interacting clusters are large. The effective charge $Z_{c,c}$ was determined in Ref. [1], and the explicit values of the effective charge for ^{6}Be and ^{12}C can be found in Refs. [34] and [37], respectively.

The asymptotic behavior of wave functions presented in Eq. (9) is formulated for the so-called 3-to-3 scattering. This approximation is valid if there are no bound states in any two-cluster subsystem. That is the case for nuclei ^{9}Be and ^{9}B we are going to study.

In closing this section, we consider possible values of the quantum numbers of hyperspherical harmonics. First, we consider possible values of the partial angular orbital momenta l_1 and l_2. They determine the total parity of a three-cluster state; $\pi = (-1)^{l_1+l_2}$. This is the first restriction on possible values of l_1 and l_2. Next, the total orbital momentum L is a vector sum of the partial angular orbital momenta l_1 and l_2: $\mathbf{L} = \mathbf{l}_2 + \mathbf{l}_2$ and thus

$$L = |l_1-l_2|,|l_1-l_2|+1,\ldots,l_1+l_2.$$

This is the second restriction. The last restriction is connected with peculiarities of the hyperspherical harmonics. For a fixed value of the hypermomentum K, a sum l_1+l_2 takes the values

$$l_1+l_2 = K_{\min},K_{\min}+2,\ldots,K,$$

where $K_{\min} = L$ is for the normal parity state $\pi = (-1)^L$, and $K_{\min} = L+1$ is for the abnormal parity state $\pi = (-1)^{L+1}$. Combing the first and third restrictions, we conclude that the hyperspherical harmonics with even values of K describe positive parity states, while the harmonics with odd values of K describe only negative parity states.

Let us consider a special case of positive parity states with the zero total orbital momentum L. In this case, the partial orbital momenta $l_1 = l_2 = 0, 1,\ldots, K/2$. For a given value of the hypermomentum K, we have got $K/2+1$ hyperspherical functions. If we take all hyperspherical harmonics with $K = 0, 2,\ldots, K_{\max}$, we involve possible channels $c = 1, 2,\ldots, N_{\rm ch}$, where $N_{\rm ch} = (K_{\max}+2)(K_{\max}+4)/8$. For an arbitrary value of the total orbital momentum L, by taking all hyperspherical harmonics with $K =$

$K_{\min}, K_{\min}+2, \ldots, K_{\max}$ into account, we will involve $N_{\rm ch} = (K_{\max}-K_{\min}+2)(K_{\max}-K_{\min}+4)(L+1)/8$ channels.

As we deal with the oscillator functions describing the three-cluster system, we will use the quantum number $N_{\rm sh}$, which enumerates oscillator shells for the state of the compound system with the parity π and the total angular momentum L. The oscillator function $|n_\rho, c\rangle$ with given values of n_ρ and K belongs to the oscillator shell

$$N_{\rm sh} = n_\rho + (K - K_{\min})/2$$

provided that $K \geqslant K_{\min}$. This condition means that if $n_\rho = 0$, the oscillator function with the hypermomentum $K = K_{\min}$ appears on the oscillator shell $N_{\rm sh} = 0$, the oscillator function with $K = K_{\min}+2$ appears on the oscillator shell $N_{\rm sh} = 1$, and so on. If $K = K_{\min}$, then the number of the oscillator shell $N_{\rm sh}$ coincides with the number of the hyper-radial excitations n_ρ. On the oscillator shells $N_{\rm sh} \geqslant (K_{\max}-K_{\min})/2$, we have got a fixed number of oscillator functions $N_f = (K_{\max}-K_{\min})/2+1$.

III. SPECTRUM OF RESONANCE STATES IN ^{9}Be AND ^{9}B

To perform numerical calculations, we need to fix a few parameters and select the nucleon-nucleon (NN) potential. We start with its selection. Here, we exploit the modified Hasegawa-Nagata potential (MHNP) [3,4]. This is an effective NN potential constructed from the realistic nuclear force, by using the reaction matrix method, and it has been intensively used for numerous many-cluster systems, as it provides a good description of the internal structure of clusters and the interaction between clusters as well. After the NN potential was selected, we need to fix four input parameters: the oscillator length b, number of channels or number of hyperspherical harmonics, and number of hyper-radial excitations.

We restrict ourselves with a finite set of hyperspherical harmonics, which is determined by the maximal value of the hyperspherical momentum $K_{\max}$. To describe the positive parity states, we use all hyperspherical harmonics with the hypermomentum $K \leqslant K_{\max} = 14$, and the negative parity states are described by the hyperspherical harmonics with $K \leqslant K_{\max} = 13$. These numbers of hyperspherical harmonics account for many different scenarios of the three-cluster decay. We also restrict ourselves with the number of hyper-radial excitations $n_\rho \leqslant 100$. This allows us to reach the asymptotic region, where all clusters are well separated, and the cluster-cluster interaction induced by the NN potential becomes negligibly small. In Table I, we collect information about the number of total channels ($N_{\rm ch}$) involved in calculations for different values of the total angular momentum J and parity π. We also indicated the number of channels compatible with the total orbital momentum $L = J-1/2$ [$N_{\rm ch}(J_-)$] and $L = J+1/2$ [$N_{\rm ch}(J_+)$]. Naturally, $N_{\rm ch} = N_{\rm ch}(J_-) + N_{\rm ch}(J_+)$. Note that the same set of hyperspherical harmonics was used in Ref. [2].

TABLE I. Number of channels involved in calculations for different states J^π of ^{9}Be and ^{9}B. $N_{\rm ch}(J_-)$ and $N_{\rm ch}(J_+)$ are explained in the text.

J^π	$1/2^-$	$1/2^+$	$3/2^-$	$3/2^+$	$5/2^-$	$5/2^+$	$7/2^-$	$7/2^+$	$9/2^+$
$K_{\max}$	13	14	13	14	13	14	13	14	14
$N_{\rm ch}(J_-)$		21	28	12	21	44	42	30	54
$N_{\rm ch}(J_+)$	29	12	21	44	42	30	30	54	36
$N_{\rm ch}$	29	33	49	56	63	74	72	84	90

Since the total spin of nuclei ^{9}Be and ^{9}B equals $S = 1/2$, the total orbital momentum L is not a good quantum number, and the state with the total angular momentum J will be presented by a combination of the states with $L = J-1/2$ and $L = J+1/2$. One may expect that the spin-orbital forces play a noticeable role in the formation of the ground and excited states in ^{9}Be and ^{9}B.

We selected a tree of the Jacobi vectors, where the first Jacobi vector **x** determines a distance between the centers-of-mass of two α particles, while the second Jacobi vector **y** indicates a distance of the valence nucleon to the center-of-mass of two α particles. With such a choice of the tree, the partial orbital momentum l_1 of the relative rotation of two α particles has only even values. As a consequence of that restriction, the number of independent hyperspherical harmonics is reduced two times, and the parity of the compound system is totally determined by the partial orbital momentum l_2, which is associated with the rotation of the valence nucleon around ^{8}Be as the two-cluster $\alpha+\alpha$ subsystem.

In the present paper, as in previous calculations [2], the oscillator length b is selected to minimize the bound state energy of an α particle, which is obtained with $b = 1.317$ fm. This allows us to describe correctly the internal structure of the α particle. If we take the original form of the MHNP, we obtain the overbounded ground state in ^{9}Be and the bound $3/2^-$ state in ^{9}B. The latter contradicts the experiments with ^{9}B. A similar situation was observed for the MP. To avoid this unphysical situation, we changed slightly the parameters of the MHNP in order to reproduce the bound state energy of ^{9}Be. We recall that a modification of the Majorana parameter affects only the odd components of the central part of the NN potential. This modification does not affect the spin-orbital components of the MHNP, which are taken in the original form. Within the present model, the odd components determine the interaction between clusters, but are not involved in determining the internal energy of each cluster consisting of s-wave configurations. Thus, by modifying the Majorana parameter, we obtain the correct value of the binding energy of ^{9}Be with $m = 0.4389$, which can be compared to the original value $m = 0.4057$. With this value of the Majorana parameter, the spectra of resonance states in ^{9}Be and ^{9}B are calculated.

A. Two-cluster subsystems

Before proceeding to the resonance states in ^{9}Be and ^{9}B, let us consider how the MHNP describes their two-cluster subsystems. By using new and original parameters of the MHNP, we calculate the spectra of resonance states in two-cluster subsystems ^{8}Be, ^{5}He, and ^{5}Li. The results of these calculations are presented in Table II. One can see that the MHNP with original parameters describes better the spectrum of the resonance states in ^{8}Be, especially the 2^+ and 4^+ resonance states. However, the NN potentials with

TABLE II. Spectrum of resonance states in ^{8}Be, ^{5}He, and ^{5}Li calculated with original (O) and modified (M) parameters of the MHNP. Energy E and width Γ are in MeV.

	J^π	O		M		Expt. [38]	
		E	Γ	E	Γ	E	Γ
^{8}Be	0^+	0.360	0.032	0.859	0.958	0.092	5.57×10^{-6}
	2^+	3.196	1.716	4.138	4.809	3.12	1.513
	4^+	11.576	2.569	14.461	6.386	11.44	≈3.500
^{5}He	$3/2^-$	−0.258		0.385	0.209	0.798	0.648
	$1/2^-$	2.307	10.195	2.335	11.927	2.068	5.57
^{5}Li	$3/2^-$	0.608	0.162	1.236	0.725	1.69	1.23
	$1/2^-$	3.194	11.986	3.235	13.903	3.18	6.60

the original and modified sets of parameters yield too wider 0^+ resonance states with a larger energy. The MHNP with the modified Majorana parameter describes better the spectra of resonance states in ^{5}He and ^{5}Li than this potential with the original value of m. However, the theoretical values of energy and width of the lowest resonance states in ^{5}He and ^{5}Li differ noticeably from experimental values. Despite these discrepancies between the calculated and experimental spectra of resonance states in two-cluster systems ^{8}Be, ^{5}He, and ^{5}Li, we are going to use the MHNP with the modified value of the parameter m to study the spectrum of three-cluster resonance states in ^{9}Be and ^{9}B compound nuclei. As is well known (see, e.g., Ref. [2] and references therein), it is impossible to reproduce properly the spectra of ^{9}Be and ^{9}B with an effective NN potential, which properly describes the structures of the two-cluster subsystems ^{8}Be, ^{5}He, and ^{5}Li.

B. Three-cluster systems

Now, we turn our attention to the spectra of ^{9}Be and ^{9}B nuclei. The results of calculations with the MHNP are presented in Tables III and IV, where we compare our results with the experimental data [39]. The results of our calculations are in fairly good agreement with available experimental data.

TABLE III. Spectra of bound and resonance states of ^{9}Be calculated with the MHNP.

J^π	Expt.		AM HHB, MHNP	
	E (MeV ± keV)	Γ (MeV ± keV)	E (MeV)	Γ (MeV)
$3/2^-$	–1.5735		–1.5743	
$1/2^+$	0.111 ± 7	0.217 ± 10	0.338	0.168
$5/2^-$	0.8559 ± 1.3	0.00077 ± 0.15	0.897	2.363×10^{-5}
$1/2^-$	1.21 ± 120	1.080 ± 110	2.866	1.597
$5/2^+$	1.476 ± 9	0.282 ± 11	2.086	0.112
$3/2^+$	3.131 ± 25	0.743 ± 55	4.062	1.224
$3/2^-_2$	4.02 ± 100	1.33 ± 360	2.704	2.534
$7/2^-$	4.81 ± 60	1.21 ± 230	4.766	0.404
$9/2^+$	5.19 ± 60	1.33 ± 90	4.913	1.272
$5/2^-_2$	6.37 ± 80	∼1.0	5.365	4.384
$7/2^+$			5.791	3.479

TABLE IV. Experimental and theoretical spectra of resonance states of ^{9}B.

J^π	Expt.		AM HHB, MHNP	
	E (MeV ± keV)	Γ (MeV ± keV)	E (MeV)	Γ (MeV)
$3/2^-$	0.277	0.000 54 ± 0.21	0.379	1.076×10^{-6}
$1/2^+$	(1.9)	≃0.7	0.636	0.477
$5/2^-$	2.638 ± 5	0.081 ± 5	2.805	0.018
$1/2^-$	3.11	3.130 ± 200	3.398	3.428
$5/2^+$	3.065 ± 30	0.550 ± 40	3.670	0.415
$3/2^+$			4.367	3.876
$3/2^-_2$			3.420	3.361
$7/2^-$	7.25 ± 60	2.0 ± 200	6.779	0.896
$9/2^+$			6.503	2.012
$5/2^-_2$	12.670 ± 40	0.45 ± 20	5.697	5.146
$7/2^+$			7.100	4.462

The energy and width of some resonance states are rather close to experimental data, for instance, parameters of the $5/2^-$ and $9/2^+$ resonance states in ^{9}Be and parameters of the $5/2^-$, $1/2^-$, and $5/2^+$ resonance states in ^{9}B.

The spectra of the ground and excited states in ^{9}Be and ^{9}B, presented in Fig. 1, where the energy is displayed as a

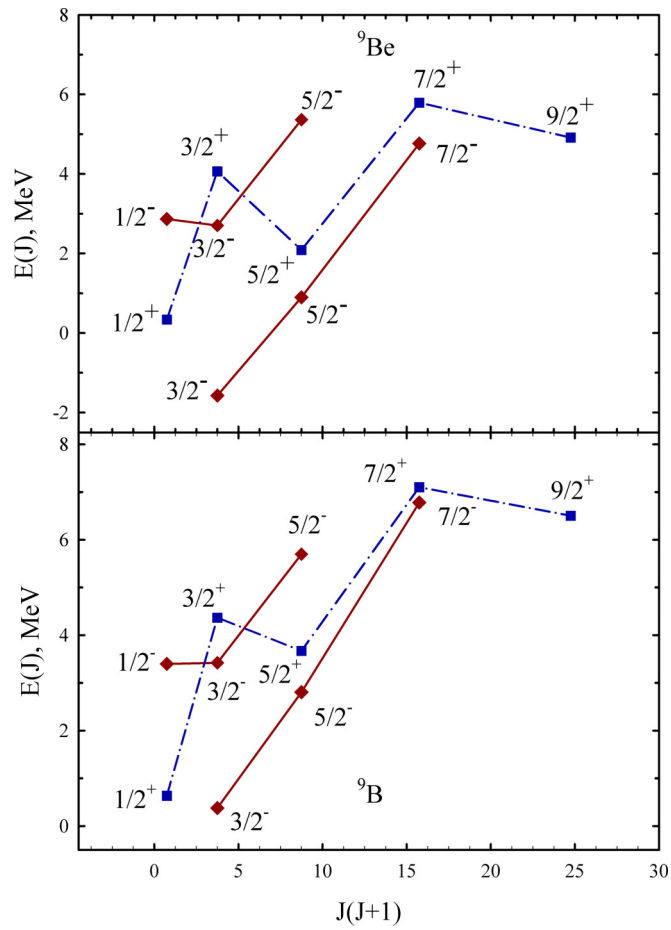

FIG. 1. Spectra of rotational bands in ^{9}Be and ^{9}B.

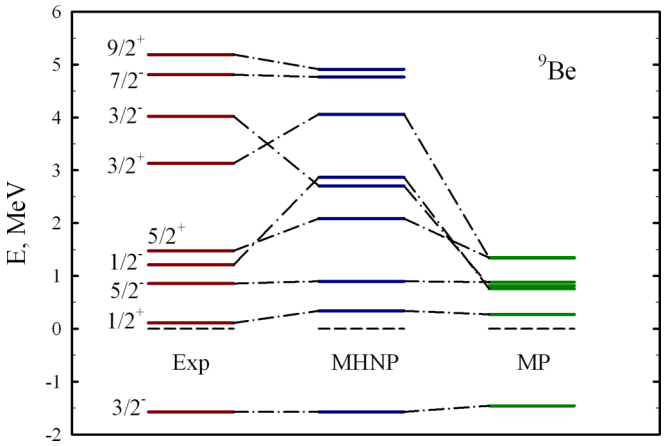

FIG. 2. Experimental (Exp) and calculated spectra of ^{9}Be determined with the MHNP and MP.

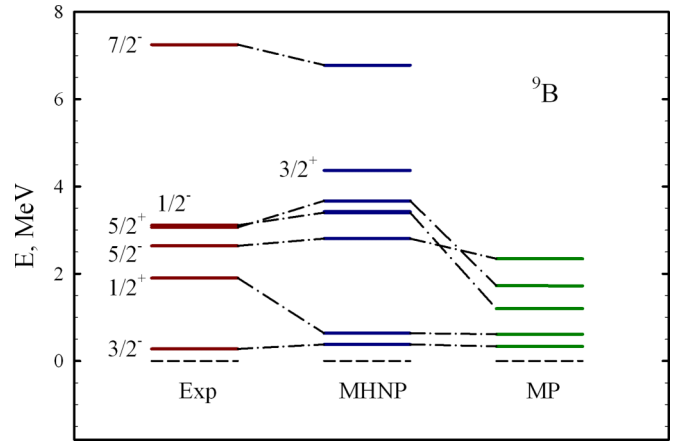

FIG. 3. Experimental and calculated spectra of ^{9}B.

function of $J(J+1)$, show that there are three rotational bands in these nuclei. They can be marked in the standard manner as $\mathcal{K}^\pi = 3/2^-$, $\mathcal{K}^\pi = 1/2^-$, and $\mathcal{K}^\pi = 1/2^+$ rotational bands. The main $\mathcal{K}^\pi = 3/2^-$ rotational bands are comprised of the $J^\pi = 3/2^-_1$, $5/2^-_1$, and $7/2^-_1$ states and are represented by almost straight lines in both nuclei. This means that the effective moment of inertia is of the rigid-body type, since it is independent of the total angular momentum J. This is the first rotational band for negative parity states. The second negative-parity rotational $\mathcal{K}^\pi = 1/2^-$ band involves also three states $J^\pi = 1/2^-$, $3/2^-_2$, and $5/2^-_2$. A bent line connects these states. However, that part of the line, which connects $3/2^-_2$ and $5/2^-_2$ states, is parallel to the line of the first rotational band. Such shape of a line in the $\mathcal{K}^\pi = 1/2^-$ band indicates that the Coriolis forces are strong in the $1/2^-$ state and are very small in the $3/2^-_2$ and $5/2^-_2$ states. The Coriolis forces, associated with the interaction of the internal and collective degrees of freedom, are rather strong in the states of the positive-parity rotational $\mathcal{K}^\pi = 1/2^+$ band. They are very strong especially for the $3/2^+$ and $9/2^+$ states, since these states strongly bend the line collecting the states of this band. For the $\mathcal{K}^\pi = 1/2^-$ band, the line connecting the $J^\pi = 5/2^+$ and $7/2^+$ states is also parallel to the line of the first rotational $\mathcal{K}^\pi = 3/2^-$ band. It is worthwhile to note a close similarity in the structures of rotational bands in ^{9}Be and ^{9}B nuclei.

In Figs. 2 and 3, we compare the results of our present calculations (MHNP) with the results of previous investigations (MP) presented in Ref. [2] and with available experimental data [39].

There are two main differences between previous calculations with the MP and new ones with the MHNP. First, the MHNP generates much less (approximately two times) of resonance states within the considered region of energy. Second, the MHNP does not create many narrow resonance states. The common feature of these two calculations is that the $1/2^+$ resonance states in ^{9}B and ^{9}Be are observed close to the three-cluster threshold $\alpha + \alpha + N$. It is worthwhile to recall that parameters of the MP and MHNP potentials were adjusted to reproduce the energy of the $3/2^-$ ground state in ^{9}Be. With these parameters, we obtained the $3/2^-$ resonance states of ^{9}B at the energy very close to the experimental one. This result means that we found the correct interaction between clusters in ^{9}B and ^{9}Be. From Figs. 2 and 3, we conclude that the MHNP generates a more correct cluster-cluster interaction for many sets of the J^π states, than the MP. We also conclude that the spectra of resonance states in ^{9}B and ^{9}Be strongly depend on peculiarities of the NN potential.

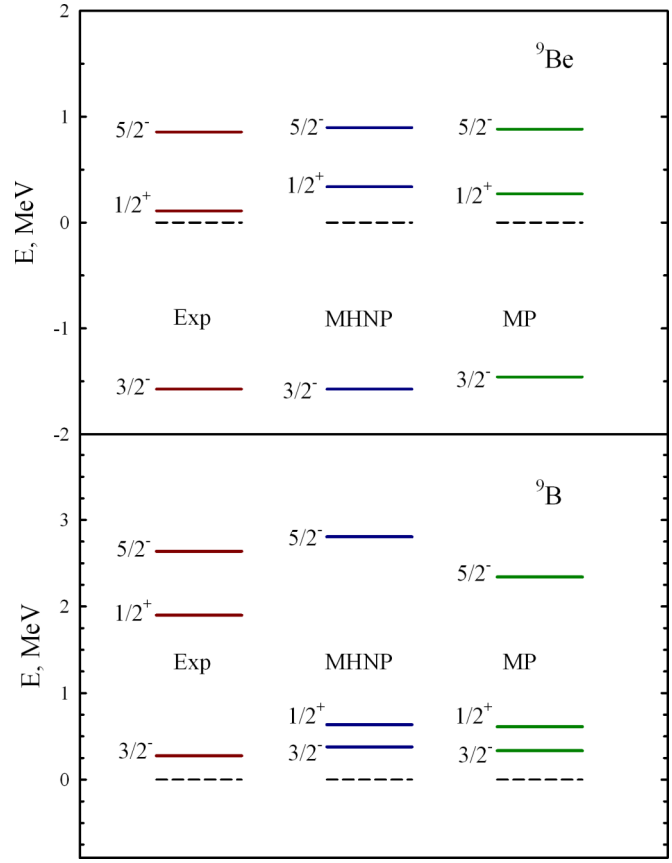

FIG. 4. Comparison of some resonance states in ^{9}Be and ^{9}B calculated with the MHNP and MP potentials and with experimental data.

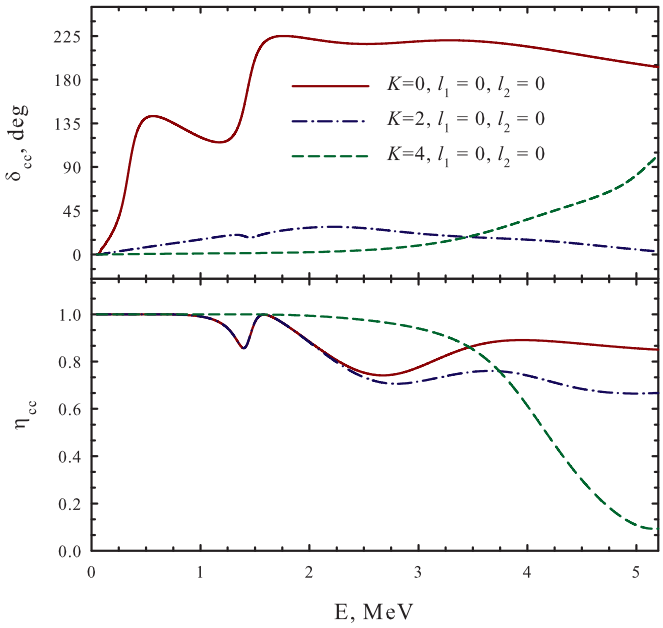

FIG. 5. Phase shifts δ_{cc} and inelastic parameters η_{cc} for the $3 \Rightarrow 3$ scattering for the $J^\pi = 1/2^+$ state in ^{9}Be.

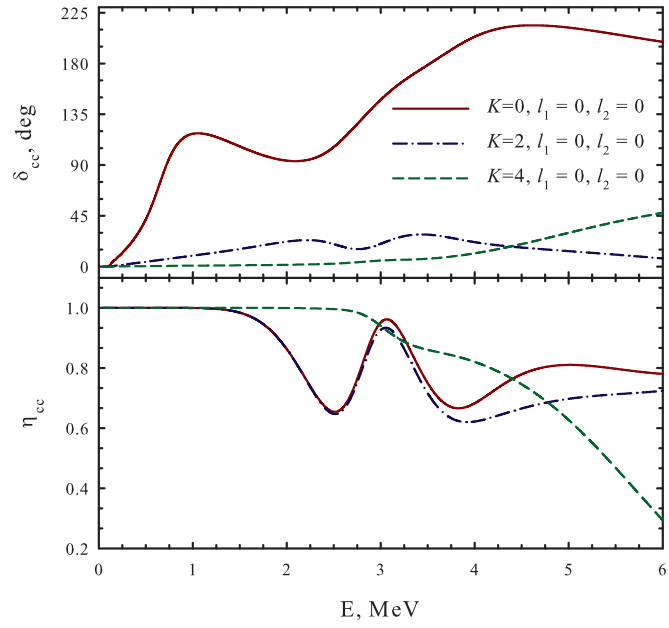

FIG. 6. Phase shifts δ_{cc} and inelastic parameters η_{cc} for the $3 \Rightarrow 3$ scattering for the $J^\pi = 1/2^+$ state in ^{9}B.

In Fig. 4, we provide a more detailed comparison of some resonance states calculated with the MHNP and MP. As we see, the positions of selected resonance states (namely $5/2^-$ and $1/2^+$ in both nuclei, and $3/2^-$ in ^{9}B) are almost independent of or slightly dependent on the shape of NN potentials.

IV. PROPERTIES OF THE $1/2^+$ RESONANCE STATES

A. Resonance solutions in the hyperspherical harmonics method

Now we turn our attention to the $1/2^+$ resonance states in ^{9}B and ^{9}Be. In this section, we are going to present more details about calculations of resonance states within the present model. Numerical solutions of the dynamic equations (8) give us $N_{\rm ch} \times N_{\rm ch}$ elements of the S matrix $\|S_{c,\tilde{c}}\|$ and a set of wave functions for a given value of energy. We analyze the behavior of the diagonal matrix elements $S_{c,c}$ of the S matrix, which are represented as $S_{c,c} = \eta_{c,c} \exp\{2i\delta_{c,c}\}$, where $\delta_{c,c}$ is the phase shift, and $\eta_{c,c}$ is the inelastic parameter. This analysis helps us to reveal resonance states and determine some of their physical properties. However, the energy of a resonance state and its total width are determined, by using the uncoupled channel or eigenchannel representation, which is obtained by reducing the scattering matrix $\|S_{c,\tilde{c}}\|$ to the diagonal form. Details of such transformations are explained in Ref. [40]. The representation allows us to calculate partial widths, to discover dominant decay channels, and thus to shed more light on the nature of investigated resonance states.

In Figs. 5 and 6, we display the diagonal phase shifts and inelastic parameters of $3 \Rightarrow 3$ scattering for the $1/2^+$ state in ^{9}B and ^{9}Be, respectively. These results are obtained with $K_{\rm max} = 14$ and with the MHNP. With such a value of $K_{\rm max}$, 33 channels are involved in calculations (see Table I) and only three of them produce phase shifts, which are not very small in the energy region $0 \leqslant E \leqslant 5$ MeV. The phase shift connected with the channel $c = \{K = 0, l_1 = 0, l_2 = 0, L = 0\}$ of ^{9}Be shows the resonance behavior at the energies $E = 0.338$ MeV and $E = 1.432$ MeV. The second resonance state is also reflected in the second channel $c = \{K = 2, l_1 = 0, l_2 = 0, L = 0\}$ as a shadow resonance. We recall that the shadow resonance appears in many-channel systems, when it is created in one channel and manifests itself in other channels. The most famous shadow resonance states are the $3/2^+$ resonance states in ^{5}He and ^{5}Li, which were thoroughly discussed in [32]. These resonance states are created by the Coulomb barrier in $d + t$ and $d + {}^3$He channels, respectively, and they are also reflected in $\alpha + n$ and $\alpha + p$ channels. If one disconnects the coupling between $d + t$ and $\alpha + n$ channels or between $d + {}^3$He and $\alpha + p$ channels, then one will observe the resonance state only in the first $d + t$ or $d + {}^3$He channel. See more detailed discussions of the shadow resonance states in Refs. [41,42].

Phase shifts δ_{cc} for the $1/2^+$ state in ^{9}B also exhibit resonance states at two energies $E = 0.636$ MeV and $E = 2.875$ MeV. As in the case of ^{9}Be, the $1/2^+$ resonance states in ^{9}B are related to only one channel,

$$c = \{K = 0,\ l_1 = 0,\ l_2 = 0,\ L = 0\}.$$

Due to the Coulomb interaction, the resonance states in ^{9}B are shifted to a higher energy region with respect to the position of these resonance states in ^{9}Be. It is worthwhile to note that one observes only elastic processes around the first $1/2^+$ resonance state in both nuclei, as the inelastic parameters $\eta_{cc} = 1$. Meanwhile, the elastic and inelastic processes are quite intense around the second $1/2^+$ resonance state in ^{9}B and ^{9}Be. These results mean that only one channel dominates in the formation of the first $1/2^+$ resonance state, and that more channels are involved in the formation and decay of the second $1/2^+$ resonance state.

Phase shifts δ_{cc} for the $1/2^+$ state in ^{9}Be and ^{9}B demonstrate that the total orbital momentum $L = 0$ dominates in this state. Can we neglect the total orbital momentum $L = 1$ to form the $1/2^+$ state? What is a role of the value of the total orbital momentum? To answer these questions, we make additional calculations by neglecting the state with $L = 1$. As a result, we obtain the $1/2^+$ resonance state in ^{9}Be with parameters $E = 0.340$ MeV and $\Gamma = 0.171$ MeV, which are close to the results with $L = 0$ and $L = 1$: $E = 0.338$ MeV and $\Gamma = 0.168$ MeV. For ^{9}B, we obtain $E = 0.649$ MeV and $\Gamma = 0.475$ MeV, which have to be compared with $E = 0.636$ MeV and $\Gamma = 0.477$ MeV. Thus, one can obtain quite correct values of energies and total widths of the $1/2^+$ resonance states in ^{9}Be and ^{9}B by omitting the $L = 1$ state.

It is worthwhile to note that, with the MHNP, we obtain the $1/2^+$ resonance states in ^{9}Be and ^{9}B with energies of 0.338 and 0.636 MeV, respectively. These energies are smaller than the energies of binary channel thresholds ^{8}Be $+ n$ and ^{8}Be $+ p$, if we take the energy of the 0^+ resonance state as the "ground state" of ^{8}Be. As we can see from Table II, this energy equals 0.859 MeV. Thus, our model with the MHNP suggests that the $1/2^+$ resonance state in ^{9}Be and ^{9}B is of the three-cluster nature. Let us compare the present result with the previous one obtained with the MP. The energies of the $1/2^+$ resonance states in ^{9}Be and ^{9}B, calculated in Ref. [2] with the MP, are equal to 0.25 and 0.59 MeV, respectively, which is higher than the energy $E = 0.17$ MeV of binary thresholds ^{8}Be $+ n$ and ^{8}Be $+ p$. Thus, the 0^+ resonance state in ^{8}Be may participate in the formation of the $1/2^+$ resonance state in ^{9}Be and ^{9}B.

B. Resonance wave functions in the oscillator shell representation

1. *Convergence of resonance energy and width*

To demonstrate that we involve a large set of the hyperspherical harmonics, which provides the convergent results for energies and widths of resonance states, we consider how they depend on the numbers of hyperspherical harmonics. In Table V, we demonstrate the convergence of parameters of the $1/2^+$ resonance states in ^{9}B and ^{9}Be. As we see, the parameters of the first $1/2^+$ resonance states in ^{9}B and ^{9}Be are quite stable, when we increase the basis of hyperspherical harmonics from $K_{max} = 4$ to $K_{max} = 14$. However, it is not the case for the second $1/2^+$ resonance states in ^{9}B and ^{9}Be, as a larger set of hyperspherical harmonics participates in the formation of these states.

TABLE V. Convergence of parameters of the $1/2^+$ resonance states in ^{9}Be and ^{9}B.

Nucleus	K_{max}	4	6	8	10	12	14
^{9}Be	E, MeV	0.338	0.338	0.338	0.338	0.338	0.338
	Γ, MeV	0.179	0.175	0.172	0.171	0.169	0.168
	E, MeV	4.972	3.710	2.091	1.886	1.764	1.432
	Γ, MeV	3.827	3.869	1.194	0.641	0.634	0.233
^{9}B	E, MeV	0.629	0.631	0.633	0.634	0.636	0.636
	Γ, MeV	0.493	0.487	0.483	0.481	0.479	0.477
	E, MeV		5.173	4.434	3.948	3.030	2.875
	Γ, MeV		3.287	3.001	3.350	1.978	1.235

TABLE VI. Total Γ and partial Γ_i widths for the second $1/2^+$ resonance states in ^{9}Be and ^{9}B.

^{9}Be												
$E = 1.432$ MeV, $\Gamma = 0.2327$ MeV												
i	K	l_1	l_2	L	Γ_i	Γ_i/Γ	K	l_1	l_2	L	Γ_i	Γ_i/Γ
1	0	0	0	0	0.1858	79.82	0	0	0	0	0.1858	79.82
2	2	0	0	0	0.0458	19.67	2	0	0	0	0.0293	12.59
3	4	2	2	0	0.0009	0.39	2	1	1	0	0.0165	7.08
4	4	2	2	1	0.0001	0.08	4	1	1	0	0.0006	0.262
5							4	2	2	0	0.0004	0.17
6							4	2	2	1	0.0001	0.05
Tree				$n + ^8$Be						^{4}He $+ ^5$He		
^{9}B												
$E = 2.871$ MeV, $\Gamma = 1.2355$ MeV												
i	K	l_1	l_2	L	Γ_i	Γ_i/Γ	K	l_1	l_2	L	Γ_i	Γ_i/Γ
1	0	0	0	0	1.1072	89.62	0	0	0	0	1.1072	89.62
2	2	0	0	0	0.1154	9.34	2	0	0	0	0.0739	5.98
3	4	0	0	0	0.0025	0.20	2	1	1	0	0.0416	3.36
4	4	2	2	0	0.0088	0.72	4	1	1	0	0.0084	0.68
5	4	2	2	1	0.0013	0.10	4	2	2	0	0.0030	0.24
6							4	1	1	1	0.0005	0.04
7							4	2	2	1	0.0008	0.07
Tree				$n + ^8$Be						^{4}He $+ ^5$He		

Our method allows one to reveal the dominant decay channels by calculating the partial widths Γ_i ($i = 1,2,\ldots, N_{ch}$, $\Gamma = \sum_{i=1}^{N_{ch}} \Gamma_i$) of each resonance state. An algorithm for their determination is presented in Ref. [40]. We consider the partial widths only of the second $1/2^+$ resonance states in ^{9}Be and ^{9}B. In Table VI, we present the total and partial widths of those channels, which make a noticeable contribution to the total width of the resonance state. In this table, we also show the ratio Γ_i/Γ in percent ($i = 1, 2,\ldots$), which explicitly indicates the most probable decay channels of the considered resonances. Note that the total contribution of the presented channels exceeds 99.95%.

In Tables VII and VIII, we collect different experimental and theoretical results concerning the parameters of the $1/2^+$ resonance states in ^{9}Be and ^{9}B. Here, the ACCCM stands for the analytic continuation in the coupling constant method [43], and GCM means the generator coordinate method [8]. Both methods make use of the same part of the Hilbert space, as we use in our model. In Ref. [8], the Volkov potential N2 supplemented with the zero-range spin-orbital interaction represents the NN potential, while the MP is involved in the ACCCM calculations [43]. The ACCCM model generates the very broad $1/2^+$ resonance states in both nuclei. The energy of each of these resonances exceeds 2 MeV. Parameters of the $1/2^+$ resonance states determined within the GCM are close to experimental values, especially for ^{9}Be. The GCM implies that the $1/2^+$ resonance state in ^{9}B is broad. Within our model, we obtain the energy of the $1/2^+$ state in ^{9}Be to

TABLE VII. Parameters of the $1/2^+$ resonance state in ^{9}Be determined by different experimental and theoretical methods.

^{9}Be			
Method	Source	E, MeV	Γ, keV
(e,e')	[44]	1.684 ± 0.007	217 ± 10
(e,e')	[29]	1.68 ± 0.015	200 ± 20
(γ,n)	[27]	1.750 ± 0.010	283 ± 42
(e,e')	[28]	1.732	270
β decay	[45]	1.689 ± 0.010	224 ± 7
(e,e')	[25]	1.748 ± 0.006	274 ± 8
(γ,n)	[46]	1.728 ± 0.001	214 ± 7
ACCCM	[43]	2.52	2620
GCM	[8]	1.55	360
AM HHB, MP	[2]	1.802	15
AM HHB, MHNP	present	1.912	168

be close to experimental data. However, its width is smaller than the experimental one. The calculated width with the MP is very small. In ^{9}B, our model generates two resonance states, one of which is close to the "ground state" ($E \approx 0.3$ MeV), and the second one has the excitation energy $E > 2$ MeV and a width around 1 MeV.

2. *Wave functions of resonance states*

To understand the nature of $1/2^+$ resonance states in ^{9}B and ^{9}Be, we analyze their wave functions. As was mentioned above, the wave function of the three-cluster system has many components and is a huge object which is difficult to be analyzed. The simplest way for analyzing the wave function of a resonance state is to study the weights of oscillator shells. In Fig. 7, we show the weights $W_{\rm sh}$ of different oscillator shells $N_{\rm sh}$ ($N_{\rm sh} = 0, 1, 2, \ldots$) in the wave function of resonance states. The weights are determined as follows:

$$W_{\rm sh} = W_{\rm sh}(N_{\rm sh}) = \sum_{n_\rho, c \in N_{\rm sh}} \left| C_{n_\rho, c} \right|^2.$$

TABLE VIII. Parameters of the $1/2^+$ resonance state in ^{9}B determined by different experimental and theoretical methods.

^{9}B			
Method	Source	E, MeV	Γ, MeV
Compilation	[26]	1.0	1.8
^{6}Li(^{6}Li,t)	[31]	0.73 ± 0.05	≈ 0.3
^{10}B(^{3}He,α)	[47]	1.8 ± 0.2	0.9 ± 0.3
^{6}Li(^{6}Li,d)	[48]	0.8–1.0	≈ 1.5
ACCCM	[43]	2.0	2.7
GCM	[8]	1.27	1.24
AM HHB, MP	[2]	0.30	0.12
AM HHB, MP	[2]	2.08	0.83
AM HHB, MHNP	present	0.26	0.48
AM HHB, MHNP	present	2.50	1.24

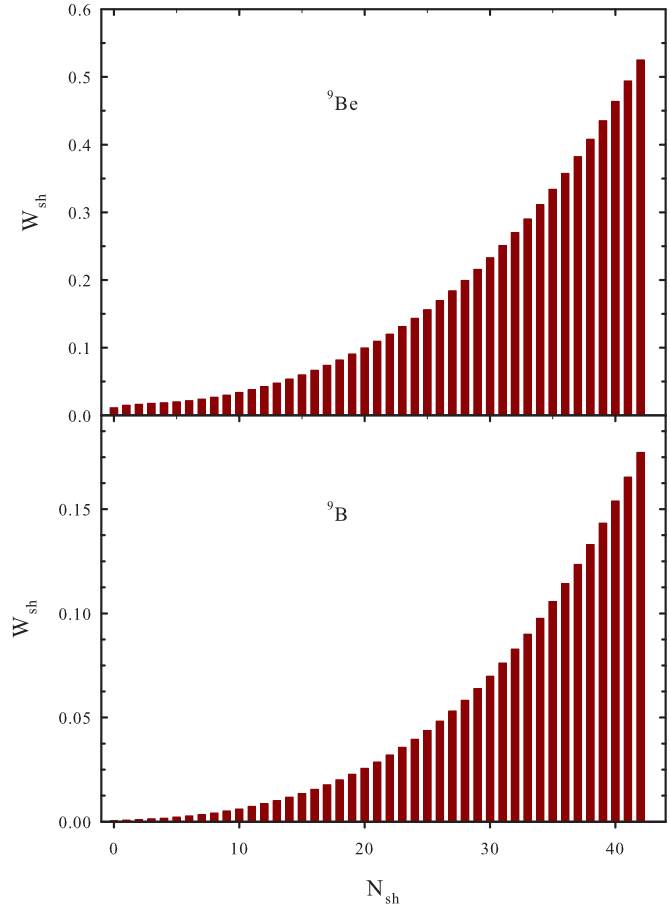

FIG. 7. Weights of different oscillator shells in the wave functions of $1/2^+$ resonance states in ^{9}Be and ^{9}B.

We note that the oscillator wave functions with small values of $N_{\rm sh}$ describe very compact configurations of the three-cluster system, when the distances between interacting clusters are very small. The oscillator functions with large values of $N_{\rm sh}$ account for configurations of the three-cluster system with large distances between all clusters, and/or if one cluster is far away from two other clusters. These statements can be deduced from the fact that the radius (or average size) of a three-cluster system, described by an oscillator function from the $N_{\rm sh}$ oscillator shell is approximately equal to $b\sqrt{4N_{\rm sh}+3}$.

We can see that the wave function of the first $1/2^+$ resonance in ^{9}Be is similar to the wave function of the first resonance state in ^{9}B, and both of them are represented by the oscillator functions with large values of the $N_{\rm sh}$ shell. Figure 7 displays the behavior of the wave function, which is typical of low-energy wave functions. In the asymptotic region, which is not shown here, these functions have an oscillatory behavior. This statement is justified by the following considerations. Like the two-body case with a sort-range interaction, the position of the first node of the wave function shifts to larger distances from the origin, as the energy decreases to zero. In the oscillator space, we have approximately the same picture, as it is seen in the coordinate space, because there is a simple relation between the wave function in the coordinate space and expansion coefficients in the oscillator representation (see

details, e.g., in [1]). To make this point clear, we consider a simple case. Suppose that we involve only one channel to describe the $1/2^+$ states in ^{9}B and ^{9}Be. This channel has the zero value of the hypermomentum. Thus, the partial orbital momenta $l_1 = l_2 = 0$, and the total orbital momentum $L = 0$. The asymptotic part of the single-channel wave function in the hyperspherical harmonic formalism [49,50] is

$$\psi_{K,=0}(\rho) \approx \frac{\cos(k\rho + \delta_0 - 5\pi/4)}{\rho^{5/2}}, \quad \rho \gg 1,$$

while the expansion coefficients in the oscillator representation are

$$C_{n_\rho K=0}(b) \approx \sqrt{2}R_n^2 \cdot \frac{\cos(kbR_n + \delta_0 - 5\pi/4)}{R_n^{5/2}}, \quad n_\rho \gg 1, \tag{12}$$

where δ_0 is the phase shift of the $3 \Rightarrow 3$ scattering with the hypermomentum $K = 0$ and

$$R_n = \sqrt{4n_\rho + 6},$$
$$k = \sqrt{\frac{2mE}{\hbar^2}}.$$

For the sake of simplicity, we assume that there is no Coulomb interaction in both ^{9}Be and ^{9}B nuclei. The expansion coefficients (12) indicate that the weight of the oscillator shell $N_{\rm sh} = n_\rho$ approximately equals

$$W_{n_\rho} \approx \left| \frac{\cos(kbR_n + \delta_0 - 5\pi/4)}{\sqrt{R_n}} \right|^2 \tag{13}$$

and tends to zero, as n_ρ goes to infinity due to the denominator proportional to $n_\rho^{1/2}$. It is seen from (13) that the oscillator shells that obey the conditions

$$kbR_n + \delta_0 - 5\pi/4 = \nu\pi/2, \quad \nu = 1,2,\ldots$$

give a negligibly small contribution to the wave function in the oscillator representation $C_{n_\rho K=0}$ and, consequently, to the weight W_{n_ρ}. One may expect a node of the wave function at this point of the discrete coordinate n_ρ.

In a more complicated case where a large number of hyperspherical harmonics are involved in calculations, one expects an oscillatory behavior of the wave functions and weights $W_{\rm sh}$ of the oscillator shells for any state of the continuous spectrum. For the states with large energies, more nodes of a wave function in the oscillator representation can be observed within a finite range of oscillator shells.

Such behavior of resonance wave functions may explain why these resonances are difficult to be detected by alternative methods.

It is worthwhile to note that such shape of the resonance wave function is observed not only for the $1/2^+$ resonance states in ^{9}Be and ^{9}B, but also for the low-lying $1/2^+$ resonances in ^{11}B and ^{11}C, as shown in Ref. [51]. These resonance states were considered as candidates for the Hoyle-analog states in ^{11}B and ^{11}C. They are narrower ($\Gamma = 12$ and $\Gamma = 163$ keV for $A = 11$ comparing to $\Gamma = 168$ and $\Gamma = 477$ keV for $A = 9$) than the $1/2^+$ resonance states in ^{9}Be and ^{9}B. However, the behavior of shell weights is very similar.

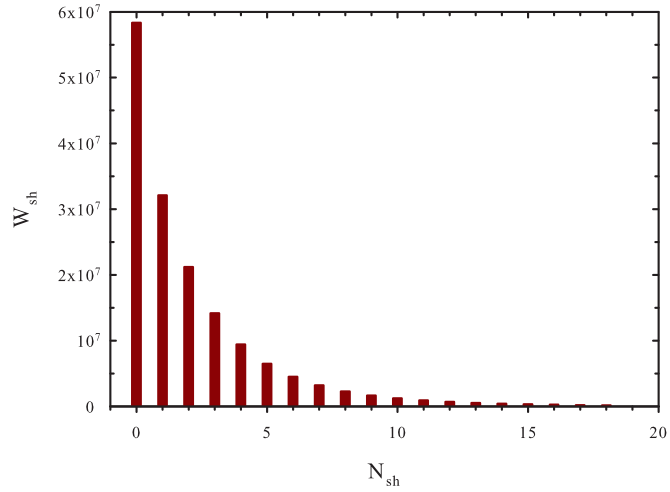

FIG. 8. Structure of the wave function of the $3/2^-$ resonance state in ^{9}B.

In Fig. 8, we show the weights $W_{\rm sh}$ for the narrow $3/2^-$ resonance state in ^{9}B. This is a typical picture for very narrow resonance states in light nuclei. There are two main features of the wave functions of narrow resonance states. First, the wave function is represented by the oscillator shells with small values of $N_{\rm sh}$. Second, it has very large values of the weights $W_{\rm sh}$ for resonance states.

It should be stressed that all wave functions of continuous spectrum states are normalized by the standard condition

$$\langle \Psi_{E,J^\pi} | \Psi_{\widetilde{E},J^\pi} \rangle = \delta(k - \widetilde{k}),$$

where

$$k = \sqrt{\frac{2mE}{\hbar^2}}, \quad \widetilde{k} = \sqrt{\frac{2m\widetilde{E}}{\hbar^2}}.$$

By analyzing the total and partial widths, we determine the dominant decay channels of a three-cluster resonance state. This analysis help us to shed some light on the nature of a resonance channel in many-channel systems. It can be performed for two different trees of the Jacobi vectors, which were denoted as $n + {}^8$Be and ^{4}He $+ {}^5$He in Ref. [2]. The $1/2^+$ resonance states in ^{9}Be and ^{9}B have only dominant channel. In the first tree $n + {}^8$Be, the resonance prefers to decay into the dominant channel, where the relative orbital momentum of two α particles and the orbital momentum of the valence neutron (with respect to the center-of-mass of two α particles) are equal to zero. The partial width of this channel almost coincides with the total width. The same situation is observed in the second tree, ^{4}He $+ {}^5$He. There is also only one dominant channel with partial orbital momenta $l_1 = 0$ and $l_2 = 0$. The first orbital momentum l_1 represents the relative motion of the neutron around the first α particle and the second one l_2 represents the relative motion of the second α particle with respect to the center-of-mass of the subsystem $\alpha + n$. These properties of the $1/2^+$ resonance states in ^{9}Be and ^{9}B are based on two important facts. The first fact is that the resonance wave functions have the dominant configuration with $K = 0$. The second fact is that the $K = 0$ hyperspherical harmonic has

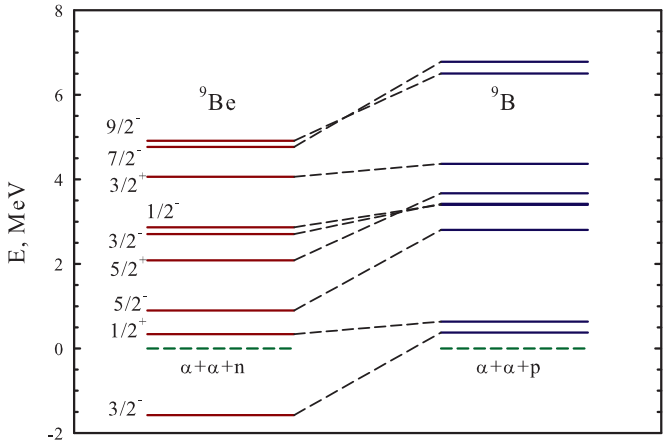

FIG. 9. Spectra of bound and resonance states in ^{9}Be and ^{9}B calculated with the MHNP.

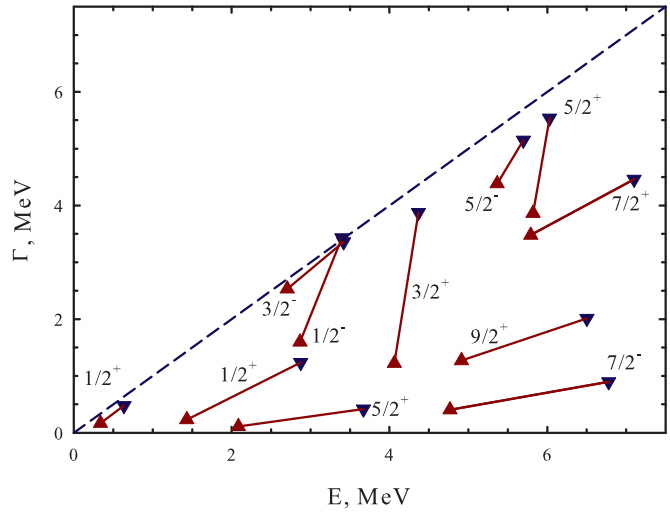

FIG. 10. Displacement of resonance states due to the Coulomb interaction.

the essential property of $l_1 = 0$ and $l_2 = 0$ independently of the Jacobi tree.

V. EFFECTS OF COULOMB FORCES

Within the present model, the differences in the positions and total widths of resonance states in mirror nuclei ^{9}Be and ^{9}B arise from the Coulomb interaction solely, which is stronger in ^{9}B, as compared with ^{9}Be.

Effects of the Coulomb interaction on mirror or isobaric nuclei have been repeatedly investigated by many researchers. Very often, the influence of the Coulomb potential on the spectra of such nuclei is associated with the Thomas-Erhman effect or shift (see, e.g., [52] and references therein), which is connected with a shift of the energy of single-particle levels in mirror nuclei due to the Coulomb interaction. By considering the mirror nuclei in the isotopic spin formalism, one can suggest twofold effects of the Coulomb forces on the parameters of resonance states. First, increasing the Coulomb interaction leads to decreasing the attractive interaction in each channel of a many-channel system. It can shift up the energies of resonance states and can also increase the widths of resonance states. Second, the Coulomb interaction makes the effective barrier wider, which can decrease both energies and widths of resonance states. What scenario is realized in nuclei ^{9}Be and ^{9}B, and how does it depend on the total angular momentum J?

A first effect of the Coulomb forces in the mirror nuclei ^{9}Be and ^{9}B can be seen in Fig. 9, where the spectra of these nuclei are shown. Five dashed lines connecting levels with the same total angular momentum J and parity π in ^{9}Be and ^{9}B show that the Coulomb forces significantly shift up levels ($J^\pi = 3/2^-$, $5/2^-$, $5/2^+$, $7/2^-$, and $9/2^-$), and four dashed lines indicate a moderate shift up of the energies of the resonance states ($J^\pi = 1/2^+$, $3/2^-$, $1/2^-$ and $3/2^+$) in ^{9}B comparing with the corresponding states in ^{9}Be.

In Fig. 10, we see how the Coulomb forces affect both energy E and width Γ of a resonance state. In this figure, the resonance states of ^{9}Be are marked by triangles up, while the resonance states of ^{9}B in the plane E-Γ are indicated by triangles down. The dashed line indicates the case $\Gamma = E$, i.e., the width of a resonance state equals its energy. As one can see from Tables III and IV and from Fig. 10, the energy of the resonance state of ^{9}Be with given total angular momentum J and parity π is lower than the analogous resonance state in ^{9}B. All resonance states in ^{9}Be are narrower than the corresponding resonance states in ^{9}B.

The results presented in Tables III and IV and in Figs. 9 and 10 indicate that just the first scenario is realized in mirror nuclei ^{9}Be and ^{9}B. The Coulomb force leads to the increase in both energies and widths of resonance states. We can separate all resonance states into three categories depending on effects of the Coulomb interaction. For this aim, we calculate the "Coulomb shift angle"

$$\theta_C = \arctan\left(\frac{E(^9\mathrm{B}) - E(^9\mathrm{Be})}{\Gamma(^9\mathrm{B}) - \Gamma(^9\mathrm{Be})}\right)$$

for each pair of resonance states in ^{9}Be and ^{9}B with given values of the total momentum J and parity π. The first category consists of resonance states with the Coulomb shift angle $40 \leqslant \theta_C \leqslant 50^\circ$. We refer to this category as a category with the moderate Coulomb effects. There are several resonance states, when the Coulomb forces increase the energy and the width in the same proportion. This leads to the case where the line connecting analogous resonance states is parallel or almost parallel to the line $\Gamma = E$. These are $1/2^+$ and $3/2^-_2$ resonance states. The second category of resonance states consists of those with the Coulomb shift angle $\theta_C < 37^\circ$. We refer to it as a category of weak Coulomb effects. In this case, the Coulomb interaction changes strongly the energy and weakly changes the resonance width. This category includes $5/2^-_1$, $5/2^+_1$, $7/2^-$, $7/2^+$, and $9/2^+$ resonance states. The third category includes the resonance states with slightly changed energy, but with strongly increased width. The Coulomb shift angle for this category $\theta_C > 66^\circ$. This category consists of four resonance states: $1/2^-$, $3/2^+$, $5/2^-_2$, and $5/2^+_2$.

Thus, the Coulomb interaction has weak, moderate, or strong influences on the parameters of resonance states in mirror nuclei ^{9}Be and ^{9}B.

VI. HOYLE-ANALOG STATES

We recall that the Hoyle state is a very narrow resonance state in ^{12}C. It lies not far from the three-cluster threshold ($E = 0.38$ MeV) and has a very small width, $\Gamma = 8.5$ eV. One of the main features of the Hoyle resonance state is that it is a very long-lived resonance state (on the nuclear scale). The Hoyle state plays an important role in the nucleosynthesis of carbon in helium-burning red giant stars, which are rich of α particles. The present AM HHB model was successfully used in Ref. [37] to study the spectra of bound and resonance states in ^{12}C. It was obtained that the Hoyle state is generated by the triple collision of three α particles. (It should be stressed that the present model accounts for both sequential and simultaneous decays or excitations of a three-cluster resonance state. Technically, it is very difficult to distinguish a sequential decay from a simultaneous one in the present approach. Thus, in our notation, the term "the triple collision" stands for both types of processes.) These results of the present model encouraged us to search the Hoyle-analog states in ^{9}Be. There is a quest for the Hoyle-analog states in light nuclei by different theoretical methods. Here, we are going to find the Hoyle-analog state(s) in ^{9}Be, by using the AM HHB model.

If we look at Table III, we find that ^{9}Be has two resonance states ($1/2^{+}$ and $5/2^{-}$), which lie close to the three-cluster threshold $\alpha + \alpha + n$. However, the $1/2^{+}$ resonance state is not a narrow one, as the ratio Γ/E is large ($\Gamma/E \approx 0.5$). Meanwhile, the $5/2^{-}$ resonance state is indeed a narrow resonance state, because its width is small $\Gamma = 23.6$ eV, and, in addition, the ratio Γ/E is also very small. It equals $\Gamma/E \approx 2.63 \times 10^{-5}$ in our model, whereas the experimental ratio is $\Gamma/E \approx 9.0 \times 10^{-4}$. One can compare this ratio with the experimental ratio $\Gamma/E \approx 2.24 \times 10^{-7}$ for the Hoyle state.

Our calculation indicates that the $5/2^{-}$ resonance state is the Hoyle-analog state. This state has a quite large half-life time, could emit quadrupole γ quanta, and transit to the ground state of ^{9}Be. This is one of the possible ways for the synthesis of ^{9}Be. We assume that, in stars with large densities of α particles and neutrons, this is a very plausible way of creating ^{9}Be nuclei.

The present model indicates also that the $1/2^{+}$ resonance state, being a too wide or too short-lived one, has very small chance to participate in the synthesis of ^{9}Be.

Let us consider the structure of the $5/2^{-}$ resonance state in ^{9}Be. In Fig. 11, we demonstrate the weights $W_{\rm sh}$ of different shells in the wave function of the $5/2^{-}$ resonance state. It can be concluded from this figure that the $5/2^{-}$ resonance state is a compact object, as it is mainly represented by the oscillator shells with small numbers of $N_{\rm sh}$. The structure of the wave function of the $5/2^{-}$ resonance is similar to that of the ^{9}Be ground-state wave function, which was displayed in Fig. 3 of Ref. [2]. In both cases, the main contribution to the wave functions of bound and resonance states comes from the oscillator shells $N_{\rm sh} \leqslant 15$. In addition, the wave function of the resonance state has a very large amplitude in the internal region ($W_{\rm sh} \leqslant 10^{6}$). Such behavior of the wave function of the $5/2^{-}$ resonance state in ^{9}Be is very similar to the behavior of the wave function of the Hoyle state in ^{12}C (see, for instance, Refs. [51,53,54]).

By comparing Figs. 8 and 11 for the resonance states $3/2^{-}$ in ^{9}B and $5/2^{-}$ in ^{9}Be, respectively, we came to the conclusion that these figures represent the standard behavior of the wave functions for narrow resonance states. This means that the wave function of a "standard" resonance state has a very large amplitude in the internal region, and this amplitude is much larger than the oscillating amplitude in the asymptotic region. This also means that three clusters spend a long time in the region, where the intercluster distances are small, and the interaction between them is strong.

Let us consider candidates to the Hoyle-analog states in ^{9}B. This nucleus, as was mentioned above, has no bound state. Thus, there is no way for creating a stable state in the triple

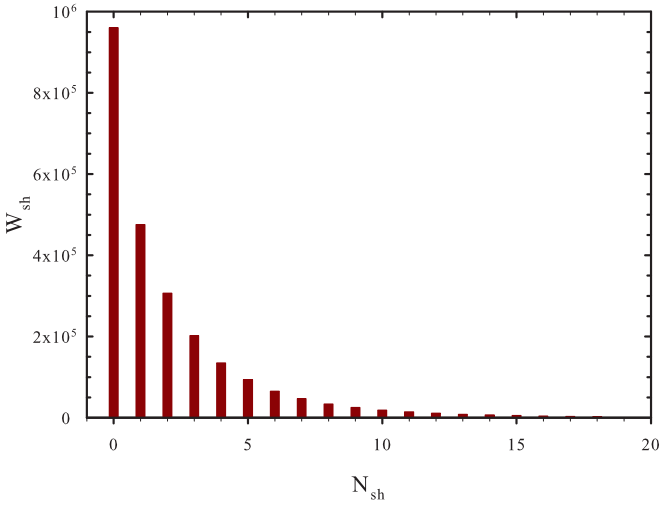

FIG. 11. Weights of different oscillator shells in the wave function of the $5/2^{-}$ resonance state in ^{9}Be.

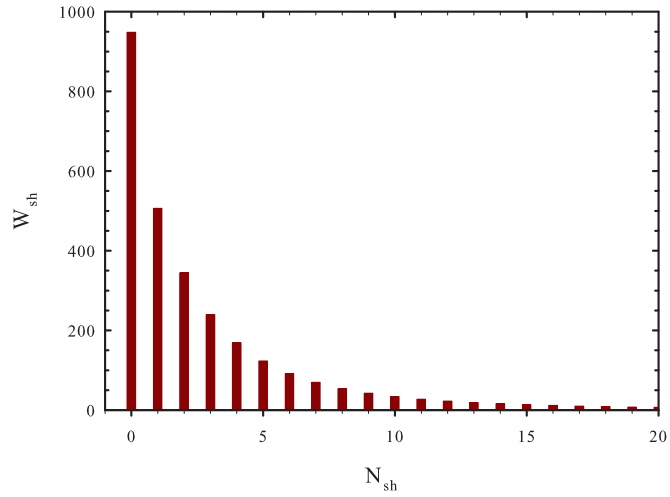

FIG. 12. Structure of the wave function of the $5/2^{-}$ resonance state in ^{9}B. The result is obtained with the MHNP.

TABLE IX. Average distances $R_1 = R(N-\alpha\alpha)$ and $R_2 = R(\alpha-\alpha)$ (in fm) for a few states of ^{9}Be and ^{9}B.

^{9}Be				
J^π	E	Γ	R_1	R_2
$3/2^-$	-1.574		3.71	3.38
$5/2^-$	0.897	2.363×10^{-5}	4.75	3.52
$1/2^+$	0.338	0.168	14.02	7.37
^{9}B				
J^π	E	Γ	R_1	R_2
$3/2^-$	0.378	1.076×10^{-6}	3.96	3.50
$5/2^-$	2.805	0.017	5.01	3.87
$1/2^+$	0.636	0.477	14.33	7.44

collision of two α particles and proton. However, one may consider the creation of a narrow resonance state in ^{9}B, which can be then transformed into a bound state of ^{9}Be by emitting a β particle or in a combination of the β and γ decays. This cascade of decays can be considered as an alternative way for the synthesis of ^{9}Be nuclei. As we see from Table IV, there are two very narrow resonance states in ^{9}B. They are the $3/2^-$ resonance state with the ratio $\Gamma/E \approx 2.8 \times 10^{-6}$ and the $5/2^-$ resonance state having the ratio $\Gamma/E \approx 6 \times 10^{-3}$. The first resonance state, as was shown in Fig. 8, is a very compact narrow three-cluster state. The $5/2^-$ resonance state in ^{9}B is not so narrow as the $3/2^-$ state. However, it has the wave function with features which are typical of narrow resonance states (see Fig. 12).

Having calculated the wave function of a bound or resonance state, we can evaluate the shape of a triangle connecting the centers-of-mass of interacting clusters. In Table IX, we display the average distances $R_2 = R(\alpha-\alpha)$ and $R_1 = R(N-\alpha\alpha)$ between clusters. The quantity $R(\alpha-\alpha)$ is the average distance between α particles, and $R_1 = R(n-\alpha\alpha)$ [or $R(p-\alpha\alpha)$] determines the average distance between the neutron (proton) and the center of mass of two α particles. It is worthwhile to note that, to calculate the average distances for resonance states, we make use of the internal part of the wave functions, which are normalized to unity (see more details in Refs. [2,51] about the definition of average distances between clusters).

The narrow resonance states indicated in Table IX have approximately the same size of the triangle as a bound state in ^{9}Be. Meanwhile, the $1/2^+$ resonance states in ^{9}Be and ^{9}B are represented by a very large triangle. We assume that such dispersed (even in the internal region) resonance states have a very small probability (comparing to the very narrow resonance states) to be transformed into a bound state.

VII. CONCLUSIONS

A three-cluster microscopic model has been applied to the studies of resonance states in mirror nuclei ^{9}Be and ^{9}B. The model makes use of the hyperspherical harmonics to enumerate the channels of three-cluster continua and to simplify the method of solution of the Schrödinger equation for many-particle many-channel systems. The MHNP is employed as the NN interaction. It is shown that the model with such NN interaction provides a fairly good description of the parameters of the known resonance states. This potential provides a much better description of the spectra of resonance states in ^{9}Be and ^{9}B than the MP, which was used in the previous paper [2]. It is shown that, within the present model, the excited $1/2^+$ states in ^{9}Be and ^{9}B are described as resonance states. It is also established that only one channel with the hypermomentum $K = 0$ dominates in the formation and decay of these $1/2^+$ resonance states. By analyzing effects of the Coulomb interaction, we have discovered three groups of resonance states, which reveal weak, medium, and strong impacts of the interaction on the energies and widths of resonance states. Our analysis leads us to the conclusion that the very narrow $5/2^-$ resonance state in ^{9}Be can be considered as the Hoyle-analog state. We assume that this state is a key resonance state for the synthesis of ^{9}Be in triple collisions of α particles and neutron in a stellar environment.

ACKNOWLEDGMENT

This work was partially supported by the Ministry of Education and Science of the Republic of Kazakhstan Research Grant No. IPS 3106/GF4. One of the authors (K.K.) acknowledges support from the JSPS KAKENHI Grants No. 25400241 and No. 17K05430

[1] V. Vasilevsky, A. V. Nesterov, F. Arickx, and J. Broeckhove, Phys. Rev. C **63**, 034606 (2001).
[2] A. V. Nesterov, V. S. Vasilevsky, and T. P. Kovalenko, Phys. At. Nucl. **77**, 555 (2014).
[3] A. Hasegawa and S. Nagata, Prog. Theor. Phys. **45**, 1786 (1971).
[4] F. Tanabe, A. Tohsaki, and R. Tamagaki, Prog. Theor. Phys. **53**, 677 (1975).
[5] P. Descouvemont, Phys. Rev. C **39**, 1557 (1989).
[6] V. T. Voronchev, V. I. Kukulin, V. N. Pomerantsev, Kh. D. Razikov, and G. G. Ryzhikh, Yad. Fiz. **57**, 1964 (1994) [Phys. At. Nucl. **57**, 1890 (1994)].
[7] K. Arai, Y. Ogawa, Y. Suzuki, and K. Varga, Phys. Rev. C **54**, 132 (1996).
[8] P. Descouvemont, Eur. Phys. J. A **12**, 413 (2001).
[9] K. Arai, P. Descouvemont, D. Baye, and W. Catford, Phys. Rev. C **68**, 014310 (2003).
[10] K. Arai, Nucl. Phys. A **738**, 342 (2004).
[11] V. D. Efros and J. M. Bang, Eur. J. Phys. A **4**, 33 (1999).
[12] M. Odsuren, Y. Kikuchi, T. Myo, M. Aikawa, and K. Katō, Phys. Rev. C **92**, 014322 (2015).
[13] Y. Kikuchi, M. Odsuren, T. Myo, and K. Katō, Phys. Rev. C **93**, 054605 (2016).
[14] B. R. Barrett, P. Navrátil, and J. P. Vary, Prog. Part. Nucl. Phys. **69**, 131 (2013).
[15] J. Carlson, S. Gandolfi, F. Pederiva, S. C. Pieper, R. Schiavilla, K. E. Schmidt, and R. B. Wiringa, Rev. Mod. Phys. **87**, 1067 (2015).
[16] S. Quaglioni and P. Navrátil, Phys. Rev. C **79**, 044606 (2009).

[17] S. Quaglioni, C. Romero-Redondo, and P. Navrátil, Phys. Rev. C **88**, 034320 (2013).
[18] C. Romero-Redondo, S. Quaglioni, P. Navrátil, and G. Hupin, Phys. Rev. Lett. **113**, 032503 (2014).
[19] P. Navrátil, S. Quaglioni, G. Hupin, C. Romero-Redondo, and A. Calci, Phys. Scr. **91**, 053002 (2016).
[20] C. Romero-Redondo, S. Quaglioni, P. Navrátil, and G. Hupin, Phys. Rev. Lett. **117**, 222501 (2016).
[21] C. Forssén, P. Navrátil, W. E. Ormand, and E. Caurier, Phys. Rev. C **71**, 044312 (2005).
[22] J. Langhammer, P. Navrátil, S. Quaglioni, G. Hupin, A. Calci, and R. Roth, Phys. Rev. C **91**, 021301(R) (2015).
[23] S. C. Pieper, K. Varga, and R. B. Wiringa, Phys. Rev. C **66**, 044310 (2002).
[24] H. Akimune, M. Fujimura, M. Fujiwara, K. Hara, T. Ishikawa, T. Kawabata, H. Utsunomiya, T. Yamagata, K. Yamasaki, and M. Yosoi, Phys. Rev. C **64**, 041305 (2001).
[25] O. Burda, P. von Neumann-Cosel, A. Richter, C. Forssén, and B. A. Brown, Phys. Rev. C **82**, 015808 (2010).
[26] R. Sherr and H. T. Fortune, Phys. Rev. C **70**, 054312 (2004).
[27] H. Utsunomiya, Y. Yonezawa, H. Akimune, T. Yamagata, M. Ohta, M. Fujishiro, H. Toyokawa, and H. Ohgaki, Phys. Rev. C **63**, 018801 (2000).
[28] F. C. Barker, Aust. J. Phys. **53**, 247 (2000).
[29] J. P. Glickman, W. Bertozzi, T. N. Buti, S. Dixit, F. W. Hersman, C. E. Hyde-Wright, M. V. Hynes, R. W. Lourie, B. E. Norum, J. J. Kelly *et al.*, Phys. Rev. C **43**, 1740 (1991).
[30] V. D. Efros, P. von Neumann-Cosel, and A. Richter, Phys. Rev. C **89**, 027301 (2014).
[31] M. A. Tiede, K. W. Kemper, N. R. Fletcher, D. Robson, D. D. Caussyn, S. J. Bennett, J. D. Brown, W. N. Catford, C. D. Jones, D. L. Watson *et al.*, Phys. Rev. C **52**, 1315 (1995).
[32] K. Wildermuth and Y. Tang, *A Unified Theory of the Nucleus* (Vieweg Verlag, Braunschweig, 1977).
[33] R. I. Jibuti and N. B. Krupennikova, *Method of Hyperspherical Functions in Quantum Mechanics of Few Body Systems* (in Russian) (Micniereba, Tbilisi, 1984).
[34] V. Vasilevsky, A. V. Nesterov, F. Arickx, and J. Broeckhove, Phys. Rev. C **63**, 034607 (2001).
[35] V. Vasilevsky, A. V. Nesterov, F. Arickx, and J. Broeckhove, Phys. Rev. C **63**, 064604 (2001).
[36] M. Abramowitz and A. Stegun, *Handbook of Mathematical Functions* (Dover, New York, 1972).
[37] V. Vasilevsky, F. Arickx, W. Vanroose, and J. Broeckhove, Phys. Rev. C **85**, 034318 (2012).
[38] D. R. Tilley, C. M. Cheves, J. L. Godwin, G. M. Hale, H. M. Hofmann, J. H. Kelley, C. G. Sheu, and H. R. Weller, Nucl. Phys. A **708**, 3 (2002).
[39] D. R. Tilley, J. H. Kelley, J. L. Godwin, D. J. Millener, J. E. Purcell, C. G. Sheu, and H. R. Weller, Nucl. Phys. A **745**, 155 (2004).
[40] J. Broeckhove, F. Arickx, P. Hellinckx, V. S. Vasilevsky, and A. V. Nesterov, J. Phys. G Nucl. Phys. **34**, 1955 (2007).
[41] B. C. Pearce and B. F. Gibson, Phys. Rev. C **40**, 902 (1989).
[42] A. Csótó, Phys. Rev. A **48**, 3390 (1993).
[43] N. Tanaka, Y. Suzuki, K. Varga, and R. G. Lovas, Phys. Rev. C **59**, 1391 (1999).
[44] G. Kuechler, A. Richter, and W. von Witsch, Z. Phys. A: At. Nucl. **326**, 447 (1987).
[45] I. Mukha, M. Kavatsyuk, A. Algora, L. Batist, A. Blazhev, J. Döring, H. Grawe, M. Hellström, O. Kavatsyuk, R. Kirchner *et al.*, Nucl. Phys. A **758**, 647 (2005).
[46] H. Utsunomiya, S. Katayama, I. Gheorghe, S. Imai, H. Yamaguchi, D. Kahl, Y. Sakaguchi, T. Shima, K. Takahisa, and S. Miyamoto, Phys. Rev. C **92**, 064323 (2015).
[47] N. Arena, S. Cavallaro, G. Fazio, G. Giardina, A. Italiano, and F. Mezzanares, Europhys. Lett. **5**, 517 (1988).
[48] T. D. Baldwin, W. N. Catford, D. Mahboub, C. N. Timis, N. I. Ashwood, N. M. Clarke, N. Curtis, V. Ziman, T. A. D. Brown, S. P. Fox *et al.*, Phys. Rev. C **86**, 034330 (2012).
[49] R. I. Jibuti and R. Y. Keserashvili, Czech. J. Phys. **30**, 1090 (1980).
[50] M. Fabre de La Ripelle, Few-Body Syst. **14**, 1 (1993).
[51] V. S. Vasilevsky, Ukr. J. Phys. **58**, 544 (2013).
[52] J. J. He and A. S. J. Murphy, Eur. Phys. J. A **34**, 315 (2007).
[53] T. Neff and H. Feldmeier, Int. J. Mod. Phys. E **17**, 2005 (2008).
[54] T. Neff and H. Feldmeier, Few-Body Syst. **45**, 145 (2009).